

Weak-noise limit of a piecewise-smooth stochastic differential equation

Yaming Chen,^{1,*} Adrian Baule,^{1,†} Hugo Touchette,^{2,3,‡} and Wolfram Just^{1,§}

¹*School of Mathematical Sciences, Queen Mary University of London, London E1 4NS, UK*

²*National Institute for Theoretical Physics (NITheP), Stellenbosch 7600, South Africa*

³*Institute of Theoretical Physics, University of Stellenbosch, Stellenbosch 7600, South Africa*

(Dated: October 10, 2013)

We investigate the validity and accuracy of weak-noise (saddle-point or instanton) approximations for piecewise-smooth stochastic differential equations (SDEs), taking as an illustrative example a piecewise-constant SDE, which serves as a simple model of Brownian motion with solid friction. For this model, we show that the weak-noise approximation of the path integral correctly reproduces the known propagator of the SDE at lowest order in the noise power, as well as the main features of the exact propagator with higher-order corrections, provided that the singularity of the path integral associated with the non-smooth SDE is treated with some heuristics. We also show that, as in the case of smooth SDEs, the deterministic paths of the noiseless system correctly describe the behaviour of the non-smooth SDE in the low-noise limit. Finally, we consider a smooth regularisation of the piecewise-constant SDE and study to which extent this regularisation can rectify some of the problems encountered when dealing with discontinuous drifts and singularities in SDEs.

PACS numbers: 02.50.-r, 05.40.-a, 46.55.+d, 46.65.+g

I. INTRODUCTION

The study of piecewise-smooth differential equations is a relatively recent topic in the field dynamical systems [1, 2, 3, 4, 5], despite their wide use in applied sciences and engineering. The dynamics generated by these equations displays many unexpected phenomena, including stick-slip transitions associated, for example, with solid friction forces [6, 7, 8, 9], and bifurcations that do not appear in the standard classification of catastrophes of smooth dynamical systems [3, 4, 5]. They also show, in the case of systems with discontinuous derivatives or forces (so-called Filippov systems [1]), multivalued solutions for a given initial condition, leading to a loss of determinism [10].

Stochastic versions of piecewise-smooth dynamical systems perturbed by noises are also used as models of physical and biological systems. Stochastic differential equations (SDEs) with piecewise-smooth drifts are commonly used, for example, in stochastic or Brownian ratchets, which serve as models of diffusion and transport in a variety of biological motors [11]. Another important class of problem concerns diffusion of solid objects on solid surfaces, which can be modelled phenomenologically using piecewise-smooth SDEs with solid friction forces [12, 13, 14, 15]. The dynamics in this case shows stick-slip transitions, as in the noiseless case, but also new features due to the noise, such as directed motion in the absence of a mean force bias [16] and noise-dependent decay of correlation functions [17]. Some of these features have been investigated experimentally in [18, 19, 20, 21].

The theory of piecewise-smooth SDEs is only in its infancy compared to its noiseless counterpart. Exact solutions for the transition probability distribution or propagator of a few simple piecewise-constant or piecewise-linear SDEs are known; see, e.g., [12, 17, 22, 23, 24, 25, 26]. Some studies have also looked at the large deviations of SDEs with discontinuous drift (so-called SDEs with discontinuous statistics) [27, 28, 29, 30]. However, from these disconnected studies it is not clear how non-smooth SDEs can be studied with techniques developed and used for smooth systems. Here, we focus on two such techniques, namely, the path integral representation of propagators and the weak-noise (also called saddle-node or instanton) approximation of these integrals [31, 32, 33]. The weak-noise limit is particularly interesting from a physical point of view because a piecewise-smooth system does not necessarily behave continuously with the magnitude of a force or noise, and may therefore behave in a non-trivial way in the limit of vanishing noise. This raises the question of the validity of the weak-noise limit for non-smooth systems.

In this paper, we address this question in a practical way by studying a simple piecewise-constant SDE, defined by

$$\dot{v}(t) = -\mu\sigma(v(t)) + \sqrt{D}\xi(t), \quad (1)$$

where $\sigma(v)$ denotes the sign of the state variable $v(t)$, μ is a positive constant, and D is the strength of the Gaussian white noise $\xi(t)$ characterised by

$$\langle \xi(t) \rangle = 0, \quad \langle \xi(t)\xi(t') \rangle = 2\delta(t-t'). \quad (2)$$

The notation $\langle \dots \rangle$ stands for the average over the noise. Physically, the SDE (1) is the simplest model of stick-slip motion where $v(t)$ represents the velocity of a solid object of unit mass sliding over a surface with solid (also called

dry or Coulomb) friction coefficient μ per unit mass [12, 13, 14, 15]. Mathematically, it is also the simplest piecewise-smooth SDE whose time-dependent propagator $p(v, t|v_0, 0)$, representing the probability density that $v(t) = v$ given the initial condition $v(0) = v_0$, is known exactly [17]. It is thus a good starting point for benchmarking results about non-smooth SDEs.

In the present case, we have

$$p(v_t, t|v_0, 0) = \frac{\mu}{D} \hat{p}\left(\frac{\mu}{D}v_t, \frac{\mu^2}{D}t \middle| \frac{\mu}{D}v_0, 0\right), \quad (3)$$

where

$$\hat{p}(x, \tau|x', 0) = \frac{e^{-\tau/4}}{2\sqrt{\pi\tau}} e^{-(|x|-|x'|)/2} e^{-(x-x')^2/(4\tau)} + \frac{e^{-|x|}}{4} \left[1 + \operatorname{erf}\left(\frac{\tau - (|x| + |x'|)}{2\sqrt{\tau}}\right) \right] \quad (4)$$

is the propagator in non-dimensional units and $\operatorname{erf}(x)$ is the error function. This propagator is obtained by explicitly solving the corresponding time-dependent Fokker-Planck equation, which in non-dimensional units has the form,

$$\frac{\partial}{\partial \tau} \hat{p}(x, \tau|x', 0) = \frac{\partial}{\partial x} \sigma(x) \hat{p}(x, \tau|x', 0) + \frac{\partial^2}{\partial x^2} \hat{p}(x, \tau|x', 0). \quad (5)$$

Taking the limit $t \rightarrow \infty$ of $p(v, t|v_0, 0)$, we obtain the stationary probability density function of Eq. (1),

$$p(v) = \frac{\mu}{2D} e^{-\mu|v|/D}, \quad (6)$$

which solves the time-independent Fokker-Planck equation [15]. Note that $p(v_t, t|v_0, 0)$ and, by extension, $p(v)$ are symmetric under the change $v_0 \rightarrow -v_0$ and $v(t) \rightarrow -v(t)$ due to the symmetric force $\sigma(v)$. Thus we can confine the analysis to the case $v_0 > 0$ without loss of generality.

In the next section, we compare these exact results, which are valid for any noise power D , with various low-noise approximations of the path integral representation of $p(v, t|v_0, 0)$ in order to test the validity and accuracy of these approximations and to discuss subtle singularities arising in the path integral when dealing with discontinuous drifts. Related path integrals were studied in [34, 35] for a non-exactly solvable model of solid friction. For the model that we consider, we will see that the weak-noise approximation gives the correct propagator at the lowest order in D , as well as its main features with higher-order corrections, provided that some heuristics are used to treat the singularities of the path integral. The higher-order corrections are able, in particular, to reproduce the short- and long-time behaviour of the propagator, as well as its tail behaviour.

To treat the singularity of the system in a more explicit and systematic way, we then consider in Sec. III a regularised version of our model, given by

$$\dot{v}(t) = -\mu \tanh\left(\frac{v(t)}{\varepsilon}\right) + \sqrt{D} \xi(t), \quad (7)$$

which recovers the original piecewise-smooth model of Eq. (1) in the limit $\varepsilon \rightarrow 0$. Although we do not have an explicit expression for the propagator of this smooth (but nonlinear) model, we show with Langevin simulations that the weak-noise approximation of the path integral, which is now well-defined and shows no singularity, reproduces the main features of the propagator at different orders of approximation, with roughly the same accuracy as for the singular model. The regularised model also allows us to obtain analytical results about the *instanton* or optimal path of the system, which is the most probable path singled out by the weak-noise approximation, and the so-called *action functional* or *quasi-potential*, obtained by approximating the propagator at the lowest order in D with the optimal path [32, 33, 36]. From these results, presented in Section IV, we are able to study the evolution of the propagator's tails in the long-time limit, and to understand the behaviour of the SDE in the noiseless limit. Conclusions drawn from these results are given in Sec. V.

II. PIECEWISE-SMOOTH MODEL

In this section, we compare the exact propagator of the piecewise-constant SDE of Eq. (1) with various approximations of the path integral representation of this propagator, so as to discuss the validity of these approximations for a non-smooth SDE. The path integral has the form

$$p(v_t, t|v_0, 0) = \int_{(v_0, 0)}^{(v_t, t)} \mathcal{D}[v] J[v] e^{-\frac{1}{4D} S^{(0)}[v]}, \quad (8)$$

and involves two terms: the action functional

$$S^{(0)}[v] = \int_0^t (\dot{v} + \mu\sigma(v(s)))^2 ds, \quad (9)$$

which is a measure of the probability of a path $\{v(s)\}_{s=0}^t$ in velocity space, and the Jacobian functional $J[v]$, which is the Jacobian of the transformation of the Gaussian white noise $\xi(t)$ to the $v(t)$ process (see Appendix A).

For non-smooth SDEs, two problems arise with the path integral (8). The first is that, since the noiseless system $\dot{v} = -\mu\sigma(v)$ admits in general piecewise-linear trajectories that are continuous but non-differentiable at points where $v(t)$ vanishes, the minimisation of the action must also be carried over these trajectories, which means that care must be taken with the \dot{v} term in $S^{(0)}[v]$. The second problem is that the Jacobian, as given in Eq. (A3) of Appendix A, is singular. For our model, we formally have

$$J[v] = \exp\left(\mu \int_0^t \delta(v(s)) ds\right), \quad (10)$$

where $\delta(v)$ is the Dirac delta function. Below we show how to treat this singular contribution and how its inclusion or non-inclusion in the saddle-point approximation of the path integral determines different orders of approximation of the propagator as $D \rightarrow 0$.

A. Zeroth-order saddle-point approximation

The lowest order approximation of the propagator $p(v, t|v_0, 0)$ is obtained in the noiseless limit $D \rightarrow 0$ by finding the path $\{v^{(0)}(s)\}_{s=0}^t$ that minimises the action $S^{(0)}[v]$ so as to write

$$p^{(0)}(v, t|v_0, 0) = N e^{-\frac{1}{4D} S^{(0)}[v^{(0)}]}, \quad (11)$$

where N is a normalisation constant. We refer to this approximation as the *zeroth-order saddle-point approximation* or SPA(0) for short. The rationale for this approximation is that, in the limit $D \rightarrow 0$, the path integral (8) is dominated by the probability of the most probable or *optimal* path $\{v^{(0)}(s)\}_{s=0}^t$ having minimal action. The Jacobian $J[v]$ can be neglected at this level of approximation, since it does not depend on D .

The Euler-Lagrange equation associated with the minimisation of $S^{(0)}[v]$ in the region $v > 0$ and $v < 0$ is simply

$$\ddot{v}^{(0)} = 0 \quad (12)$$

and leads to straight paths

$$v_d^{(0)}(s) = (v_0 - v_t)s/t + v_0, \quad (13)$$

which we call *direct paths*. As mentioned above, in addition to these paths, we must consider paths that follow the attractor $v = 0$, since these paths appear in the noiseless system. As a result, the minimisation of $S^{(0)}[v]$ must be carried out over all continuous and piecewise-linear paths consisting of direct paths and paths following the $v = 0$ axis. This situation differs from smooth SDEs, for which the minimisation is generally over all continuously differentiable paths, and leads us to define two important heuristic principles for dealing with non-smooth SDEs: (i) the action of a path must be evaluated as the sum of the actions of all its linear (or in general smooth) parts without regard to its joining (non-smooth) points, (ii) any part of a path on the $v = 0$ axis (or, in general, on an attractor of the noiseless system) must have a zero action, in analogy with smooth systems.

In the present model, two types of optimal paths arise from the action minimisation. The first consists of direct paths $v_d^{(0)}(s)$, found above, which directly link the positive initial velocity v_0 to a final velocity v_t (see Fig. 1(a)), and whose action is

$$S^{(0)}[v_d^{(0)}] = \begin{cases} (v_t - v_0 + \mu t)^2/t - 4\mu v_t & \text{if } v_t < 0 \\ (v_t - v_0 + \mu t)^2/t & \text{if } v_t > 0. \end{cases} \quad (14)$$

The second type of paths are the piecewise linear paths mentioned above, consisting of two straight lines in the region $v > 0$ or $v < 0$ connected by a straight line at $v = 0$. The equation of these *indirect paths* is

$$v_{ind}^{(0)}(s, t_1, t_2) = \begin{cases} (t_1 - s)v_0/t_1 & \text{if } s < t_1 \\ 0 & \text{if } t_1 < s < t_2 \\ (s - t_2)v_t/(t - t_2) & \text{if } s > t_2, \end{cases} \quad (15)$$

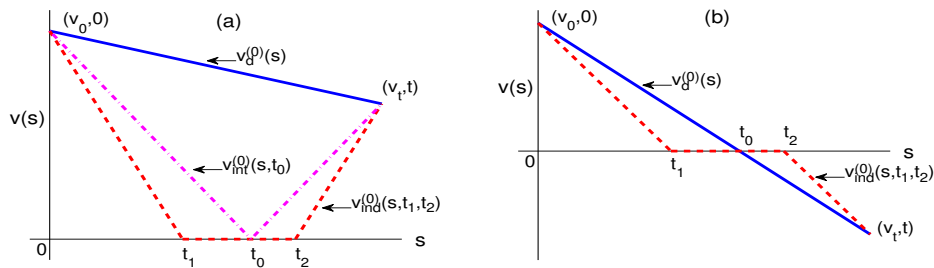


FIG. 1: (Color online) Different paths considered for minimising the action, Eq. (9), for (a) $v_t > 0$ and (b) $v_t < 0$. $v_d^{(0)}$: direct path, Eq. (13), $v_{ind}^{(0)}$: indirect path, Eq. (15), $v_{int}^{(0)}$: intermediate path, Eq. (15) with $t_1 = t_2 = t_0$.

where $t_1 < t_2$ are arbitrary times at which a path reaches $v = 0$ (see Fig. 1). Following the two principles above, we evaluate the action of these paths in a piecewise way with $S^{(0)}[0] = 0$ and minimise it for $t_1 < t_2$ to obtain

$$S^{(0)}[v_{ind}^{(0)}] = 4\mu|v_t| \quad (16)$$

for $t_1 = v_0/\mu$ and $t_2 = t - |v_t|/\mu$. Since we require $t_1 < t_2$, the lower bound is reached if $|v_t| < \mu t - v_0$. Note that paths arising in the limit case where $t_1 = t_2 \equiv t_0$ with $v_0 v_t < 0$ corresponds to direct paths, whereas those that just “bounce” on the $v = 0$ axis, i.e., $t_1 = t_2 \equiv t_0$ but $v_0 v_t > 0$ are called *intermediate paths* (see Fig. 1(a)) and have an action equal to

$$S^{(0)}[v_{int}^{(0)}] = (|v_t| + v_0 - \mu t)^2/t + 4\mu|v_t|, \quad (17)$$

for $t_0 = v_0 t / (v_0 + |v_t|)$.

It can be easily checked that any piecewise-linear paths other than those considered above have a greater action, and so cannot be optimal. Therefore, combining Eqs. (14), (16) and (17) we can write the equation of the optimal path as

$$v^{(0)}(s) = \begin{cases} v_d^{(0)}(s) & \text{if } t < v_0/\mu \\ v_{ind}^{(0)}(s, v_0/\mu, t - |v_t|/\mu) & \text{if } t > v_0/\mu \text{ and } v_t \in [v^-(t), v^+(t)] \\ v_d^{(0)}(s) & \text{if } t > v_0/\mu \text{ and } v_t \notin [v^-(t), v^+(t)], \end{cases} \quad (18)$$

where the limits of the velocity interval are defined by

$$v^-(t) = v_0 - \mu t, \quad v^+(t) = (\sqrt{v_0} - \sqrt{\mu t})^2. \quad (19)$$

This shows that, if the endpoint (v_t, t) lies in the area bounded by $v^-(s)$ and $v^+(s)$ with $s > v_0/\mu$, as shown in Fig. 2, then the optimal path is an indirect path, otherwise it is a direct path. Intermediate paths do not enter in this result, but will be useful when we treat the Jacobian.

The SPA(0) approximation of the propagator is obtained from this result by substituting the corresponding action in (11). For $t < v_0/\mu$, we find

$$p^{(0)}(v_t, t|v_0, 0) = N_1 \begin{cases} \exp(-(v_t - v_0 + \mu t)^2/(4Dt) - \mu v_t/D) & \text{if } v_t < 0 \\ \exp(-(v_t - v_0 + \mu t)^2/(4Dt)) & \text{if } v_t > 0, \end{cases} \quad (20)$$

whereas for $t > v_0/\mu$, we find

$$p^{(0)}(v_t, t|v_0, 0) = N_2 \begin{cases} \exp(-(v_t - v_0 + \mu t)^2/(4Dt) - v_t/D) & \text{if } v_t < v^-(t) \\ \exp(-(v_t - v_0 + \mu t)^2/(4Dt)) & \text{if } v_t > v^+(t) \\ \exp(-\mu|v_t|/D) & \text{if } v_t \in [v^-(t), v^+(t)], \end{cases} \quad (21)$$

where N_1 and N_2 are normalisation factors. This result is compared in Fig. 3 with the exact propagator. There we see that SPA(0) is a good approximation of $p(v, t|v_0, 0)$ at short and long times, but does not capture the bimodal structure of the propagator arising when the optimal path hits the origin for times close to $t = v_0/\mu$. While a kink

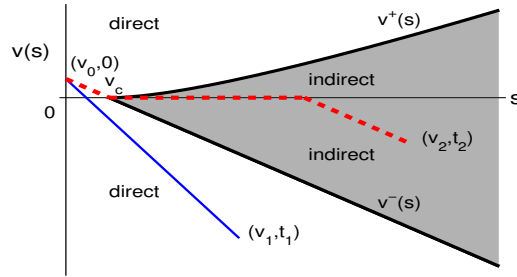


FIG. 2: (Color online) Regions in the $v_t - t$ plane for which the optimal path of the action at leading order, Eq. (9), is given by an indirect/direct path (shaded/white); see Eqs. (19). Here $v_c = \mu/v_0$ denotes the tip of the region.

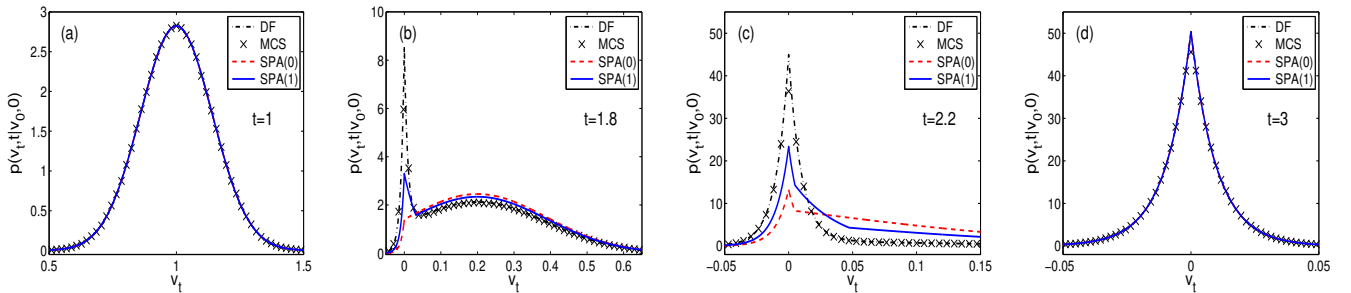


FIG. 3: (Color online) Propagator of the dry friction model (1) for initial velocity $v_0 = 2$, $\mu = 1$, $D = 0.01$ and different values of time: (a) $t = 1$, (b) $t = 1.8$, (c) $t = 2.2$, and (d) $t = 3$. DF: exact analytical result, Eq. (3), MCS: Monte Carlo simulation of Eq. (1) with step-size 0.0001 and an ensemble of 10^6 realisations, SPA(0): leading order saddle node expansion (see Eqs. (20) and (21) in Sec. II A), SPA(1): higher order saddle node expansion (see Eqs. (25), (27) and (29) in Sec. II B).

of the exact propagator shows up at time $t < v_0/\mu$ in the region $v_t > 0$ (see Fig. 3(b)), the corresponding kink of the SPA(0) only appears at time $t > v_0/\mu$; see Fig. 3(c) as well as Eqs. (20) and (21). For comparison, we also show in Fig. 3 the result of the propagator obtained from Langevin simulations of the SDE using the standard Euler-Maruyama integration scheme. The application of this scheme is stable for the piecewise smooth SDE and only requires that we choose the integration time step small enough, so that we can reproduce the cusp seen in its propagator.

We will see in the next subsection that the inclusion of the Jacobian in the saddle-point approximation enables us to reproduce this bimodality more accurately. An important remark, before we get to that part, is that the SPA(0) yields the same approximation as that obtained from the Freidlin-Wentzell (FW) large deviation theory of dynamical systems perturbed by noise [36]. Indeed, it is not difficult to verify that the limit

$$I(v, t | v_0, 0) = \lim_{D \rightarrow 0} -4D \ln p(v, t | v_0, 0) = \lim_{D \rightarrow 0} -4D \ln \hat{p} \left(\frac{\mu}{D} v_t, \frac{\mu^2}{D} t \left| \frac{\mu}{D} v_0, 0 \right. \right), \quad (22)$$

which defines in the FW theory the so-called *pseudo-* or *quasi-potential* $I(v, t | v_0, 0)$, is equal to the SPA(0) action. This shows that the application of the FW theory to non-smooth SDEs can be done following the heuristic principles formulated above. In this case, the different optimal paths that we have found can be associated, in the low-noise limit, to two different physical modes of motion of the noiseless system: direct paths represent slip motion, whereas indirect paths represent stick motion [34, 35]. For any fixed value of v_t , the optimal path will always be an indirect path if the time is sufficiently large, which means that all optimal paths are indirect paths in the limit $t \rightarrow \infty$.

B. Corrected action

One way to correct the SPA(0) is to use the optimal paths obtained before but to evaluate their action by including the Jacobian in the action:

$$S[v] = \int_0^t [(\dot{v} + \mu\sigma(v))^2 - 4D\mu\delta(v)] ds. \quad (23)$$

This defines a first-order saddle-point approximation, referred to as SPA(1), of the propagator that retains the optimal paths of SPA(0) but includes the subdominant correction of the Jacobian, which is multiplied by D .

To obtain this approximation, we need to evaluate how the contribution arising from the δ function in Eq. (23) changes the action for the different paths considered. For direct paths, there is obviously only a contribution when the $v = 0$ axis is crossed, so that

$$\int_0^t \delta(v_d^{(0)}) ds = \begin{cases} t/|v_0 - v_t| & \text{if } v_t < 0 \\ 0 & \text{if } v_t > 0. \end{cases} \quad (24)$$

Thus, the corresponding corrected action is

$$S[v_d^{(0)}] = \begin{cases} (v_t - v_0 + \mu t)^2/t - 4\mu v_t - 4D\mu t/(v_0 - v_t) & \text{if } v_t < 0 \\ (v_t - v_0 + \mu t)^2/t & \text{if } v_t > 0. \end{cases} \quad (25)$$

For intermediate paths, the evaluation of the Jacobian term is straightforward as well. Any sensible representation of the δ function will result in a symmetric average of the inverse slopes of the path, leading to

$$\int_0^t \delta(v_{int}^{(0)}) ds = \frac{1}{2|\dot{v}_{int}^{(0)}(t_0^-, t_0)|} + \frac{1}{2|\dot{v}_{int}^{(0)}(t_0^+, t_0)|} = \frac{t}{v_0 + |v_t|}, \quad (26)$$

where we have used the condition $t_0 = v_0 t / (v_0 + |v_t|)$. Hence, it follows from Eqs. (23) and (26) that

$$S[v_{int}^{(0)}] = (|v_t| + v_0 - \mu t)^2/t + 4\mu|v_t| - 4D\mu t/(v_0 + |v_t|). \quad (27)$$

Indirect paths require a closer inspection: these paths vanish over an entire interval of time, so that the contribution originating from the Jacobian is ill defined. To treat this, we follow the previous principle that paths on the attractor do not contribute to the action and posit the following two additional heuristic principles: (iii) parts of indirect paths on the attractor are not considered as contributing to the Jacobian, (iv) non-vanishing parts of indirect paths contribute, as for intermediate paths, to the Jacobian in a weighted average way. With these principles, the corrected action of indirect paths is finite and equal to

$$\int_0^t \delta(v_{ind}^{(0)}) ds = \frac{1}{2|\dot{v}_{ind}^{(0)}(t_1^-, t_1, t_2)|} + \frac{1}{2|\dot{v}_{ind}^{(0)}(t_2^+, t_1, t_2)|} = \mu, \quad (28)$$

where we have used the conditions $t_1 = v_0/t$ and $t_2 = t - |v_t|/\mu$. Thus, the corresponding action (23) can be evaluated as

$$S[v_{ind}^{(0)}] = 4\mu|v_t| - 4D\mu \quad \text{if } t > (v_0 + |v_t|)/\mu. \quad (29)$$

By properly comparing the corrected actions (25), (27) and (29), we can determine which path is minimal depending on v_t and t to obtain the propagator $p^{(0;1)}(v, t|v_0, 0)$ (see Eq. (A8)). The result of this minimisation is shown in Fig. 3 as SPA(1). We see that the inclusion of the Jacobian correction qualitatively improves the propagator as compared to the lowest order approximation, SPA(0) of Sec. II A, even though there are still some deviations in the transient regime where the exact propagator shows a bimodality. Especially, at time $t < v_0/\mu$ the SPA(1) has already shown up the kink corresponding to that of the exact propagator in the region $v_t > 0$; see Fig. 3(b). This phenomenon is different with that of the SPA(0), which does not have such a kink at $t < v_0/\mu$. We also observe in Fig. 3(c) that the SPA(1) develops two kinks in the region $v_t > 0$ in an intermediate time interval. These kinks are caused by the intermediate path which becomes the optimal path for certain choices of the endpoints. The SPA(0), by contrast, has only one kink in the positive region, since for this approximation intermediate paths can never be the optimal path; see Eq. (18). These kinks are a well-known artifact of low-noise approximations and are smoothed in the exact propagator by the finite diffusion.

C. Corrected action with corrected path

The SPA(1) corrects the SPA(0) by including the Jacobian term in the action, while using the optimal paths of SPA(0), i.e., the paths that minimise the zeroth-order action $S^{(0)}[v]$. As a further correction to this approximation, it is tempting to obtain the optimal paths by minimising the corrected action $S[v]$ with the Jacobian, thereby constructing a “full” first-order approximation.

Unfortunately, this approach does not work as the action turns out to diverge for $v_t = 0$. To see this, evaluate the action of Eq. (23) for an intermediate path $v_{int}^{(0)}$ with a kink at $t_0 = t/2$ (see Fig. 1):

$$S[v_{int}^{(0)}] = 2\mu(|v_t| - v_0) + \mu^2 t + 2(v_0^2 + v_t^2)/t - D\mu(t/v_0 + t/|v_t|). \quad (30)$$

This value is an upper bound for the minimum of the action, which determines the density according to Eq. (A10). The problem with this result is that $S[v_{int}^{(0)}] \rightarrow -\infty$ when $v_t \rightarrow 0$, leading to a (non-integrable) singularity for the propagator $p(v_t, t|v_0, 0)$ at $v_t = 0$. Thus the approximation scheme based on obtaining the optimal paths from $S[v]$ results in a non-normalisable expression, which implies that a “full” first-order SPA is not possible for the SDE of Eq. (1). It is clear that this problem will also arise in any SDE having, as in Eq. (1), points where the force of the SDE is discontinuous. One way to approach this problem is to explore regularisations of such discontinuities.

III. REGULARISED SDE

As seen in the previous section, the weak noise expansion of the path integral for non-smooth SDEs faces some difficulties related to the minimisation of the action and the singularity of the Jacobian term. To treat this problem, we now consider the regularised SDE of Eq. (7) in which the discontinuous drift $\sigma(v)$ is replaced by the smooth drift $\tanh(v/\varepsilon)$ involving the additional (small) parameter ε . For this smooth SDE, the aforementioned difficulties do not occur: we can minimise the action over smooth differentiable paths and the Jacobian is well defined. In this section, we are interested in understanding the weak noise properties of this regularised SDE.

To investigate the regularised model, we introduce non-dimensional units:

$$u = v/\varepsilon, \quad \tau = \mu t/\varepsilon. \quad (31)$$

Equation (7) is then simply written as

$$\dot{u} = -\tanh(u) + \sqrt{\tilde{D}}\xi(\tau), \quad (32)$$

where $\tilde{D} = D/(\varepsilon\mu)$ is now the only parameter of the model, called the effective diffusion constant. An important point to note is that the two limits $\varepsilon \rightarrow 0$ and $D \rightarrow 0$ do not commute. In the following, we will be interested in the smooth model for small and moderate effective noise amplitudes.

As mentioned in the introduction, the propagator of the regularised model does not have a known closed analytic form. Thus, for benchmarking the weak noise expansion results, we need to resort to numerical simulations obtained with the Euler-Maruyama scheme [37], which accurately reproduce, as for the piecewise smooth SDE, all the features of the propagator, provided that we choose the integration time step small enough.

As before, the leading order of the weak noise expansion of Eq. (32) is determined by the action (see Eqs. (A5) and (A7))

$$S^{(0)}[u] = \int_0^\tau (\dot{u}(s) + \tanh u(s))^2 ds \quad (33)$$

evaluated for the solution of the Euler-Lagrange boundary value problem (see Eq. (A6))

$$\ddot{u}^{(0)}(s) = \tanh(u^{(0)}(s))/\cosh^2(u^{(0)}(s)), \quad u^{(0)}(0) = u_0, \quad u^{(0)}(\tau) = u_\tau. \quad (34)$$

The leading order may be improved by taking consistently first-order contributions into account. The propagator (A10) is then determined by the action (see Eq. (A4))

$$S[u] = \int_0^\tau \left((\dot{u}(s) + \tanh u(s))^2 - 2\tilde{D}/\cosh^2(u(s)) \right) ds \quad (35)$$

evaluated at the path of order one which obeys the boundary value problem (A9)

$$\ddot{u}^{(1)}(s) = (1 + 2\tilde{D}) \tanh(u^{(1)}(s))/\cosh^2(u^{(1)}(s)), \quad u^{(1)}(0) = u_0, \quad u^{(1)}(\tau) = u_\tau. \quad (36)$$

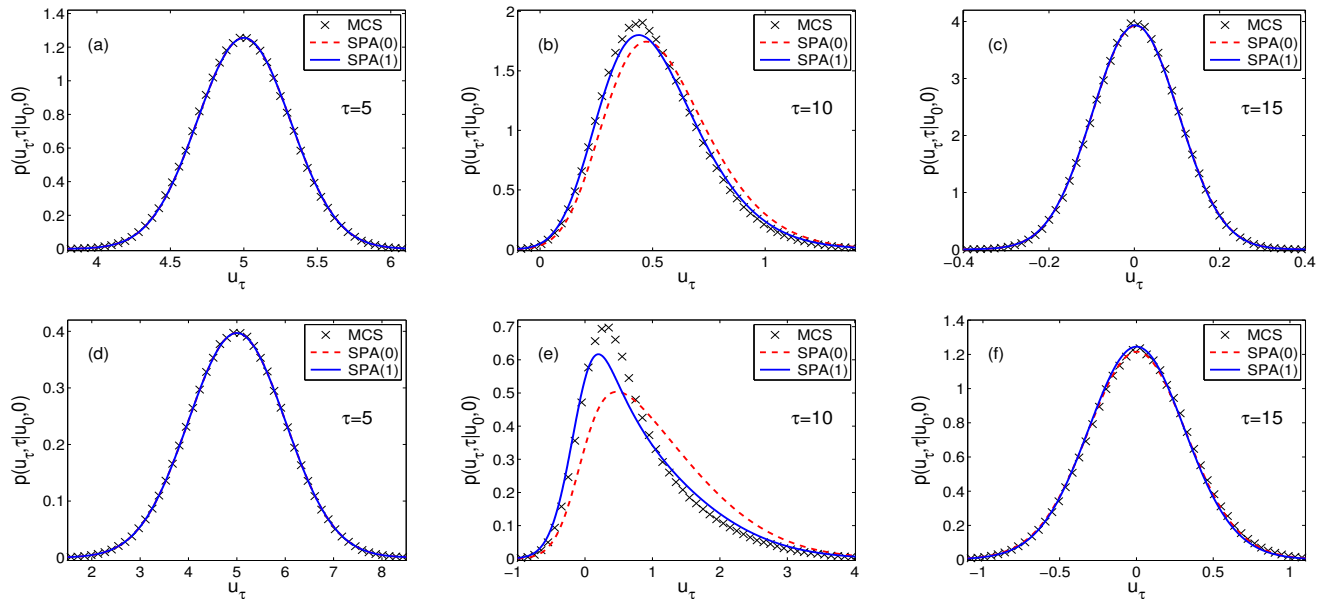


FIG. 4: (Color online) Propagator of Eq. (32) for small and moderate values of the effective diffusion, $\tilde{D} = 0.01$ ((a)-(c)) and $\tilde{D} = 0.1$ ((d)-(f)), initial condition $u_0 = 10$ and three different values of τ . MCS: Monte Carlo simulations of the Langevin equation (32) with time step 0.005 and an ensemble of 10^6 realisations, SPA(0): lowest order of the saddle node expansion using the action of Eq. (33), see Eq. (A7), SPA(1): first order of the saddle node expansion using the action of Eq. (35); see also Eq. (A10).

The two boundary value problems (34) and (36) just differ by a rescaling of time, and can be solved using a numerical shooting method (see Appendix A).

Fig. 4 compares the numerical Monte Carlo simulations of Eq. (32) with the zero- and first-order weak noise approximations for small and moderate noise amplitudes. We see that, while the short and long time behaviours are captured quite well by the lowest order approximation, substantial transient deviations are visible when the maximum of the propagator approaches the origin. The first order approximation is in fact able to deal with such a feature, even for substantial noise amplitudes. Thus, the scheme outlined above can be considered as a candidate to deal with the weak noise limit even in systems which mimic the discontinuous drift.

Naturally, from our study of the discontinuous model, we cannot expect the weak noise approximation to yield the full propagator of the smooth model in the asymptotic limit $\varepsilon \rightarrow 0$. However, it should be possible to obtain, at a quantitative level, the main features of the propagator for suitable small values of D and ε . Of course, an improved scheme such as the first-order expansion needs to be applied, as one cannot rely on extremely small values of the effective diffusion to cover cases which are sufficiently close to a discontinuous drift. Indeed, Fig. 5 shows that this is the case if we translate the results obtained via Eqs. (35) and (36) to the dimensional units via Eq. (31). The SPA(1) performs well in short time and is also able to capture the main profiles of the piecewise smooth SDE in moderate and long times. Larger deviations between the discontinuous and the regularised result appear only in a neighbourhood of size ε of the discontinuity. Hence, we may conclude that, in these particular cases, a suitable regularisation and first-order saddle point approximation are able to capture the essential features of the piecewise smooth SDE.

To close this section, let us comment on the kinks appearing in the quasi-potential, corresponding to the minimized action. These non-analytic points are well known in large deviation theory to arise from the non-uniqueness of the solutions of the Euler-Lagrange boundary value problem [38]. Since Eqs. (34) and (36) only differ by a rescaling of time, and since we are here mainly concerned with the essential structure of the quasi-potential we just focus on the simple zero order expansion, Eqs. (33) and (34). Fig. 6 shows the solution of the boundary value problem using the shooting method for a given value of u_0 . At some finite value of τ , the boundary value problem develops a cusp singularity, beyond which three solutions occur in a finite interval of u_τ values, corresponding to smooth versions of the previously-identified direct, indirect and intermediate paths. Hence, we recover in the smooth model the same path structure of the discontinuous model.

A non-unique solution to the boundary value problem implies that the actual optimising path has to be determined from minimising Eq. (33) among the three possible paths. In our case, Fig. 6 shows that the optimal path is either

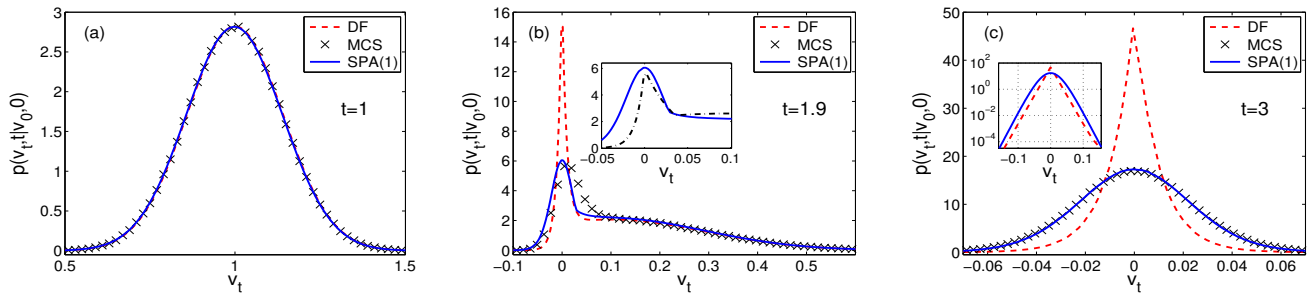


FIG. 5: (Color online) Comparison of the propagators of the dry friction model, Eq. (1) and of the regularised scheme, Eq. (7) for $\mu = 1$, $D = 0.01$, $\varepsilon = 0.05$, initial condition $v_0 = 2$ and three different values of time: (a) $t = 1$, (b) $t = 1.9$, and (c) $t = 3$. DF: Analytical result for the propagator of the dry friction model, see Eq. (3). MCS: Monte Carlo simulation of the Langevin equation (7) with time-step 0.005 and an ensemble of 10^6 realisations, SPA(1): first order saddle node approximation scheme using the action of Eq. (35). The inset in (b) shows the SPA(1) of the smooth case (full line) and the SPA(1) of the dry friction case (broken line, see Eqs. (25), (27), and (29)). Both of these graphs have a kink which matches the structure appearing in the exact solution of the dry friction model (DF). The inset in (c) shows the data for DF and SPA(1) on a larger scale in a semi-logarithmic plot. Large quantitative deviations appear only in a neighbourhood of size ε of the discontinuity.

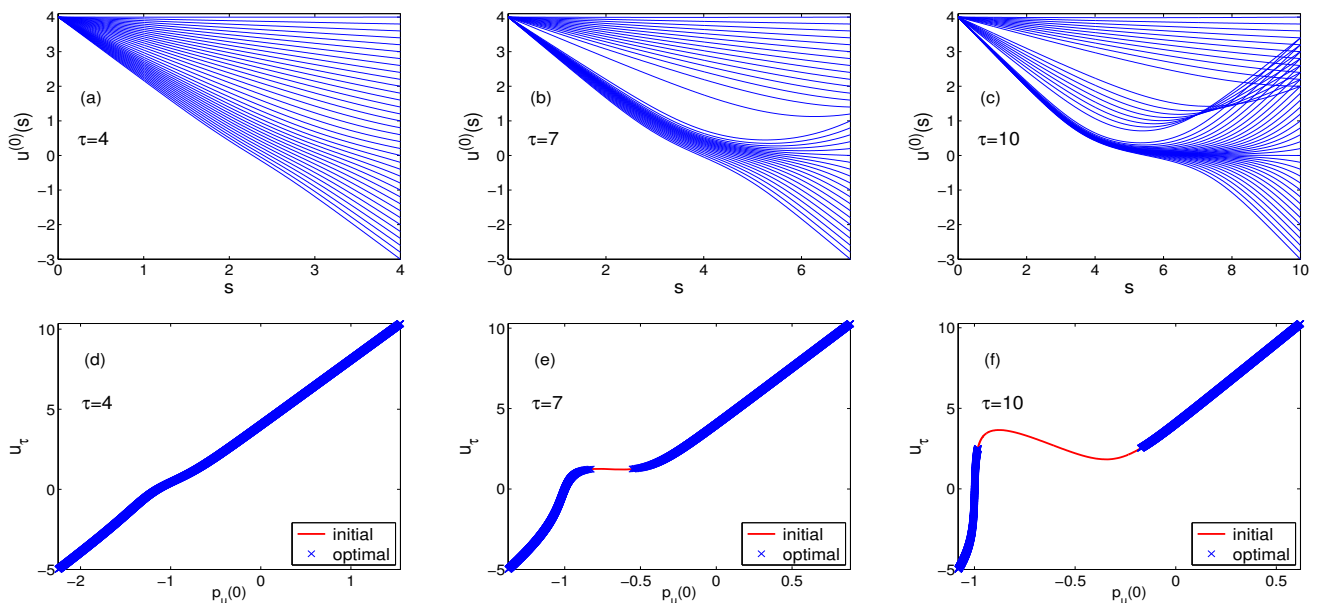


FIG. 6: (Color online) Solution of the boundary value problem (34) with the shooting method for the given value $u_0 = 4$ and three different values of τ . (a)-(c): Solutions of the differential equation (34) for different values of the initial slope $\dot{u}^{(0)}(0) = p_u(0)$. (d)-(f): Dependence of the final value $u_\tau = u^{(0)}(\tau)$ on the initial condition $\dot{u}^{(0)}(0) = p_u(0)$ of the differential equation (34), indicated by the solid line. The symbols indicate the solution which minimises the action (33).

a direct or an indirect path, as for the piecewise constant SDE. The intermediate path is always a saddle point of the action, which implies that the quasi-potential consists of two analytic branches, with a kink appearing when the type of optimal paths changes (see Figs. 5(b) and 7(b,c)). The kink, which also shows up in the numerical solution of the Fokker-Planck equation, is an important feature of the quasi-potential: it appears at finite time and then moves to larger u_τ values (see Fig. 7(c)). This feature, which is related to the convergence of the propagator towards the stationary distribution, is studied in detail next.

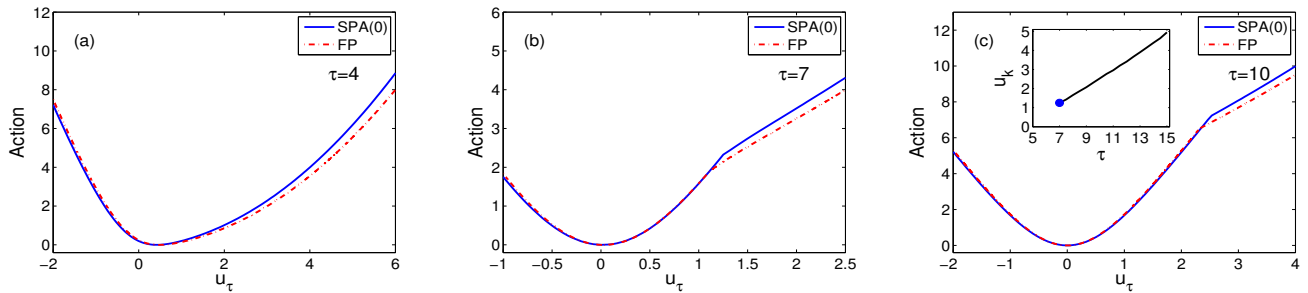


FIG. 7: (Color online) Quasi-potential of the regularised model, Eq. (32), for initial condition $u_0 = 4$, $D = 0.0001$ and three different values of time: (a) $\tau = 4$, (b) $\tau = 7$, and (c) $\tau = 10$. FP (broken line): potential $-4D \ln p(u_\tau, \tau | u_0, 0)$ computed by numerical integration of the Fokker-Planck equation. SPA(0) (full line): result of the leading order SPA, i.e., minimised action (33). The inset in (c) shows the position of the kink, u_k , as a function of the time τ , as obtained from SPA(0). The filled circle shows the time and the position where the kink emerges; see also Fig. 12.

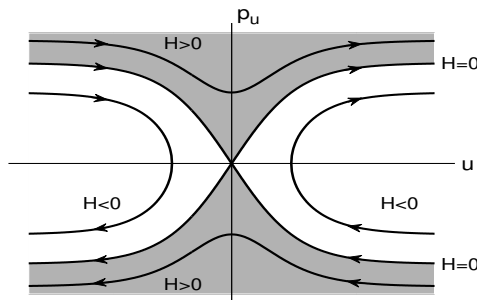


FIG. 8: Phase portrait of the Hamiltonian system Eq. (37) which governs the boundary value problem (34). The region of positive energy is shaded.

IV. ANALYTIC PROPERTIES OF THE ACTION

The previous analysis was mainly based on a numerical solution of the boundary value problem (34) and the evaluation of the corresponding action integral (33) (see [39] for a related numerical study). In this section, we try to obtain further insights into the weak noise limit by studying some analytical properties of the quasi-potential, focusing on the zeroth-order approximation of the action. The first-order approximation of the action can be analysed along similar lines.

A. Action integral

The Euler-Lagrange equations (34) are equivalent to a conservative system with Hamiltonian

$$H(p_u, u) = \frac{1}{2}p_u^2 - \frac{1}{2}\tanh^2(u), \quad (37)$$

where $p_u = \dot{u}$. The phase portrait of this system, shown in Fig. 8, is important to understand the structure of the boundary value problem. The origin in phase space is a hyperbolic equilibrium point. Regions of positive and negative energy, respectively, are bounded by the separatrix of this fixed point. Solutions of the equation of motion (34) are given by constant energy levels

$$\dot{u} = p_u = \pm \sqrt{\tanh^2(u) + 2H}, \quad (38)$$

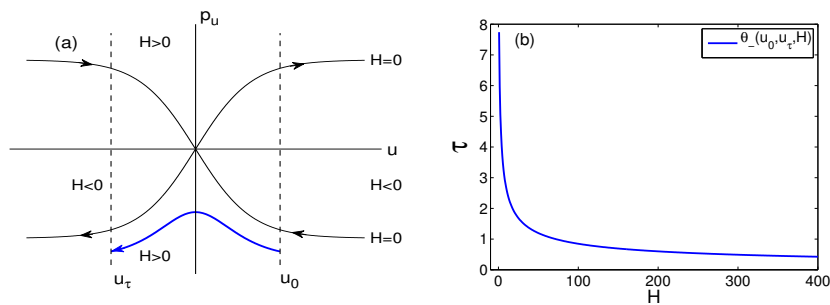


FIG. 9: (Color online) (a): Phase portrait of the Hamiltonian (37) with an orbit connecting two boundary points $u_\tau < 0 < u_0$ at a given energy $H > 0$. (b): Energy time relation, Eq. (41) for $u_0 = 10$ and $u_\tau = -2$.

where the sign determines whether the path is in the positive or negative momentum region of phase space. The zero order action (33) for a path with energy H , starting at u_0 and terminating at u_τ can then be written as

$$S^{(0)}[u] = S(u_0, u_\tau, \tau, H) = 2 \int_{u_0, H}^{u_\tau} p_u(s) du(s) + 2 \ln \left(\frac{\cosh(u_\tau)}{\cosh(u_0)} \right) - 2H\tau \quad (39)$$

if we take the expression (37) for the Hamiltonian into account. The duration τ of this path from u_0 to u_τ is evaluated as

$$\tau = \int_{u_0, H}^{u_\tau} \frac{du(s)}{p_u(s)}, \quad (40)$$

and allows us to express the energy in Eq. (39) in terms of the time. Thus the problem has been reduced to evaluating two integrals and solving algebraic equations. To take care of the correct sign in Eq. (38), we have to distinguish three cases, according to the sign of the terminal point u_τ .

1. Case 1: $u_\tau < 0 < u_0$

As can be seen from the phase portrait of Fig. 9(a), there is for given energy $H > 0$ a unique path connecting the two boundary points. Along this path Eq. (38) holds with a minus sign, and the expression relating energy and time, Eq. (40), results in

$$\tau = \int_{u_\tau}^{u_0} \frac{du}{\sqrt{\tanh^2(u) + 2H}} = \theta_-(u_0, u_\tau, H), \quad (41)$$

where

$$\theta_-(u_0, u_\tau, H) = \frac{1}{\sqrt{1+2H}} \ln \left(\frac{\sinh(u_0) + \sqrt{2H/(1+2H) + \sinh^2(u_0)}}{\sinh(u_\tau) + \sqrt{2H/(1+2H) + \sinh^2(u_\tau)}} \right). \quad (42)$$

It is easy to show that in the range $H > 0$ and $u_\tau < 0 < u_0$, Eq. (42) is a monotonic decreasing function of H (see Fig. 9(b)), i.e., Eq. (41) defines the energy H as an analytic expression of τ and of the boundary points (see Appendix B 1). As for the integral which enters the action (39) we obtain

$$\int_{u_0, H}^{u_\tau} p_u(s) du(s) = \int_{u_\tau}^{u_0} \sqrt{\tanh^2(u) + 2H} du = \int_{u_\tau}^{u_0} \frac{1 + 2H - 1/\cosh^2(u)}{\sqrt{\tanh^2(u) + 2H}} du = (1 + 2H)\tau - \sigma_-(u_0, u_\tau, H), \quad (43)$$

where we have introduced the abbreviation

$$\sigma_-(u_0, u_\tau, H) = \ln \left(\tanh(u_0) + \sqrt{2H + \tanh^2(u_0)} \right) - \ln \left(\tanh(u_\tau) + \sqrt{2H + \tanh^2(u_\tau)} \right). \quad (44)$$

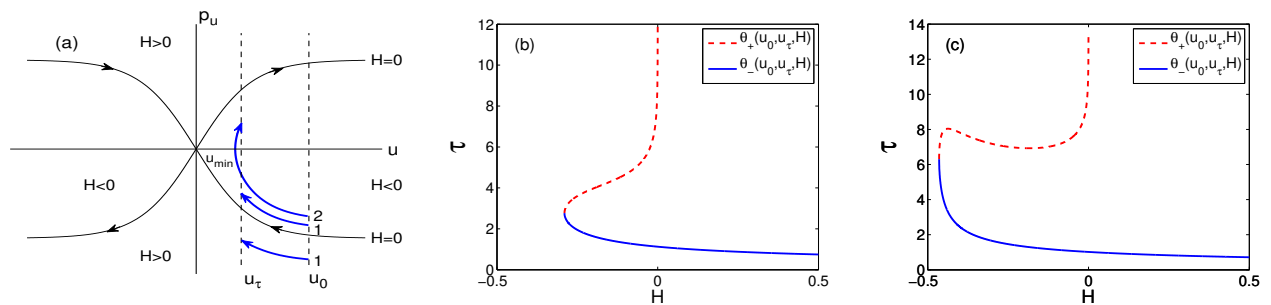


FIG. 10: (Color online) (a): Phase portrait of the Hamiltonian (37) with direct (1) and indirect (2) paths connecting boundary points $0 < u_\tau < u_0$. (b): Energy time relation, Eqs. (41) (solid line) and (46) (broken line) for small values of u_0 ($u_0 = 2$, $u_\tau = 1$) with unique inverse. (c): Energy time relation, Eqs. (41) (solid line) and (46) (broken line) for larger values of u_0 ($u_0 = 3$, $u_\tau = 2$) with multivalued inverse in a finite time interval.

Therefore the entire action, Eq. (39), finally reads

$$S(u_0, u_\tau, \tau, H) = 2(1 + H)\tau + 2 \ln \left(\frac{\cosh(u_\tau)}{\cosh(u_0)} \right) - 2\sigma_-(u_0, u_\tau, H). \quad (45)$$

Since the boundary value problem has a unique solution, the inverse of the energy-time relation (41) is single valued, so that the expression for the action defines an analytic expression of time τ and of the boundary points in the region $u_\tau < 0 < u_0$ (see as well Fig. 7).

2. Case 2: $0 < u_\tau < u_0$

For boundary points $0 < u_\tau < u_0$ the phase portrait 10(a) and Eq. (37) show that the connecting path has energy $H > H_{min} = -\tanh^2(u_\tau)/2$. On the one hand, for energies $H > H_{min}$, there exists a direct path whose duration is given by Eq. (41) and whose action is determined by Eq. (45). On the other hand, for $H_{min} < H < 0$, there exists an indirect path with a turning point at $u_{min} = \operatorname{artanh}(\sqrt{-2H})$. The duration of this path is obtained from Eq. (40) by splitting the path into two parts and using appropriate signs in Eq. (38):

$$\tau = \int_{u_0}^{u_{min}} \frac{du}{-\sqrt{\tanh^2 u + 2H}} + \int_{u_{min}}^{u_\tau} \frac{du}{\sqrt{\tanh^2 u + 2H}} = \theta_+(u_0, u_\tau, H), \quad (46)$$

where

$$\theta_+(u_0, u_\tau, H) = \frac{\ln \left(\sinh(u_0) + \sqrt{2H/(1+2H) + \sinh^2(u_0)} \right)}{\sqrt{1+2H}} + \frac{\ln \left(\sinh(u_\tau) + \sqrt{2H/(1+2H) + \sinh^2(u_\tau)} \right)}{\sqrt{1+2H}} + \frac{\ln((1+2H)/(-2H))}{\sqrt{1+2H}}. \quad (47)$$

Similarly, the integral appearing in the action (39) can be evaluated (see Eq. (43))

$$\int_{u_0, H}^{u_\tau} p_u(s) du(s) = - \int_{u_0}^{u_{min}} \sqrt{2H + \tanh^2(u)} du + \int_{u_{min}}^{u_\tau} \sqrt{2H + \tanh^2(u)} du = (1+2H)\tau - \sigma_+(u_0, u_\tau, H), \quad (48)$$

where we have introduced the abbreviation

$$\sigma_+(u_0, u_\tau, H) = \ln \left(\tanh(u_0) + \sqrt{2H + \tanh^2(u_0)} \right) + \ln \left(\tanh(u_\tau) + \sqrt{2H + \tanh^2(u_\tau)} \right) - \ln(-2H). \quad (49)$$

Thus, for the action (39) of this path we obtain

$$S(u_0, u_\tau, \tau, H) = 2(1 + H)\tau + 2 \ln \left(\frac{\cosh(u_\tau)}{\cosh(u_0)} \right) - 2\sigma_+(u_0, u_\tau, H). \quad (50)$$

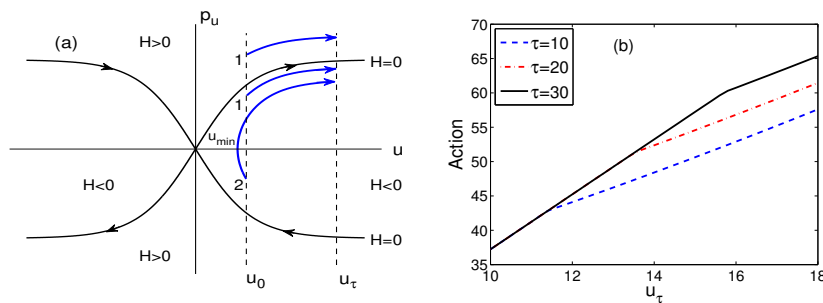


FIG. 11: (Color online) (a): Phase portrait of the Hamiltonian (37) with direct (1) and indirect (2) orbits connecting boundary points $0 < u_0 < u_\tau$. (b): Minimal action (39) as a function of u_τ in the interval $u_\tau > u_0 = 10$ for different values of the time τ , showing a kink moving to the right.

To find the minimising path, we have to take a closer look at the energy-time relation. This relation consists of two branches (see Fig. 10(b) and (c)). The branch determined by Eq. (41) is defined for all energies $H_{min} < H$ and is a monotonic decreasing function for $0 < u_\tau < u_0$ (see Appendix B 1). The second branch, defined for negative energies only, $H_{min} < H < 0$ is given by Eq. (46). This branch is monotonic increasing for small values of u_0 and develops an inflection point if the boundary points exceed a critical value, which implies that, for small values of u_0 , the relation determines the energy in terms of time and boundary points uniquely. This uniqueness is expected, as the analysis of the regularized model reduces, in the limit of small value of u_0 , to that of the Ornstein-Uhlenbeck process. However, if the initial condition is beyond the linear regime, the energy time relation has a multivalued inverse within a finite time interval (see Fig. 10(c)). The value of the action entering in the propagator is then the minimum among the three possible inverse values. The data show that for fixed values of u_0 and u_τ the minimum is given by the low energy solution, i.e., by the direct path, up to a critical value of τ while the minimum for larger values of τ is given by the high energy solution, i.e. the indirect path. The intermediate path, i.e., the solution with energy in between, is always of saddle type. As a consequence, the action, considered as a function of u_τ switches the analytical branch and develops a kink (see Figs. 7(b,c) and 11(b)).

3. Case 3: $0 < u_0 < u_\tau$

As in the previous case there are two types of paths to consider: in the energy range $H > H_{min} = -\tanh^2(u_0)/2$, there exists a direct path connecting the two boundary points, while for negative energies, $H_{min} < H < 0$, there exist in addition indirect paths with a turning point at $u_{min} = \text{artanh}(\sqrt{-2H})$. This is similar to case 2 and the relevant integrals can be dealt with by applying the symmetry of the phase portrait (see Fig. 11(a)). To find the duration of the direct path, Eq. (40), we just observe that by swapping the boundary points and reversing the direction of the path we obtain a corresponding mirror orbit with the same duration, which we have dealt with in the previous paragraph. Thus Eq. (41) tells us that

$$\tau = \int_{u_0}^{u_\tau} \frac{du}{\sqrt{\tanh^2 u + 2H}} = \theta_-(u_\tau, u_0, H). \quad (51)$$

Since the integral of the action has the same symmetry, we obtain the result stated in Eq. (43) by swapping u_0 and u_τ on the right-hand side. Thus the action (39) finally reads

$$S(u_0, u_\tau, \tau, H) = 2(1 + H)\tau + 2 \ln \left(\frac{\cosh(u_\tau)}{\cosh(u_0)} \right) - 2\sigma_-(u_\tau, u_0, H). \quad (52)$$

The action itself does not share the aforementioned symmetry because of the additional terms appearing in Eq. (39).

For the indirect path the same reasoning applies. The duration of the path, given by Eq. (46) applies, since the right hand side is symmetric in u_0 and u_τ and swapping both arguments does not have any effect. In fact, the same argument is valid for the integral which enters the action. Therefore, Eq. (48) holds, since the right hand side is a symmetric expression in the boundary points, and the corresponding action is indeed given by Eq. (50).

Overall, we see that the energy-time relationship is at the heart of understanding the structure of the optimal paths, the minimised action, and finally the propagator of the SDE. As in the previous case, the relation consists of two

branches (see Figs. 10(b) and 10(c)). The lower branch is given by the direct path, Eq. (51), which is a monotonic decreasing function on its domain $H > H_{min}$. The second branch for negative energies $H_{min} < H < 0$ is determined by Eq. (46) and thus largely the discussion of the previous section applies. If the initial condition is small, so that no cubic singularity appears for $0 < u_\tau < u_0$ (case 2), then such a singularity will finally develop for sufficiently large value of u_τ resulting in a non analytic minimised action. If, on the contrary, u_0 is so large that the occurrence of the kink has already happened in the domain $0 < u_\tau < u_0$, then the kink just propagates to larger values of u_τ (see Fig. 11(b)).

B. Asymptotics of the action

The analytic expressions derived in the previous section allow us to study in some detail the properties of the propagator shown, e.g., in Fig. 7. Of particular relevance is the approach to the stationary state, the tail behaviour of the distribution, and the emergence and dynamics of non-analyticities of the quasi-potential.

1. Approach to equilibrium

To study the convergence of the propagator towards the stationary distribution, we consider a fixed value of u_0 and u_τ and take the asymptotic limit $\tau \rightarrow \infty$. It is obvious from the phase portrait or from the energy-time relation, see Figs. 9(b) and 10(b), that the asymptotic limit implies $H \rightarrow 0$. Hence the energy-time relation is determined by Eq. (41) or (46), depending on the sign of u_τ . In both cases, a straightforward expansion yields

$$\tau = \ln(2 \sinh(u_0)) + \ln(-\sinh(u_\tau)/H) + \mathcal{O}(H \ln |H|). \quad (53)$$

For the action, either Eq. (45) or (50) applies, depending on the sign of u_τ , yielding the expansion

$$S(u_0, u_\tau, \tau, H) = 2(1 + H)\tau + 2 \ln \left(\frac{\cosh(u_\tau)}{\cosh(u_0)} \right) - 2(\ln(2 \tanh(u_0)) + \ln(-\tanh(u_\tau)/H)) + \mathcal{O}(H). \quad (54)$$

By solving Eq. (53) to leading order for H , Eq. (54) yields, as expected, the potential of the stationary distribution (see also Eq. (A7))

$$S(u_0, u_\tau, \tau, H) = 4 \ln \cosh(u_\tau) + \mathcal{O}(\tau \exp(-\tau)). \quad (55)$$

The full action as well as the propagator at finite time depends on the initial condition u_0 and hence does not have a symmetry with respect to u_τ . However, the stationary action and the corresponding stationary distribution is independent of u_0 , see Eq. (55) in the limit $\tau \rightarrow \infty$. In that limit the symmetry under the change $u_\tau \rightarrow -u_\tau$ is restored (see as well Eq. (6)). Above all, the saddle point expansion preserves all the symmetries of the underlying equations of motion. As for the transient properties it is easy, though more tedious, to compute the subleading term in Eq. (55) which then quantitatively describes the relaxation process.

2. Tail behaviour of the propagator

To investigate the action for large values of arguments, we consider the asymptotic limit $|u_\tau| \rightarrow \infty$ for fixed values of the time τ and initial condition u_0 , which implies, from the phase portraits of Figs. 9(a) and 11(a), $H \rightarrow +\infty$. The energy-time relation is determined by Eqs. (41) and (51), depending on the sign of u_τ , and a direct expansion results in the expression

$$\tau = \frac{1}{\sqrt{1 + 2H}} (|u_\tau - u_0| + \mathcal{O}(H^{-1})), \quad (56)$$

which is valid irrespective of the sign of u_τ . This expression is easily inverted to obtain

$$1 + 2H = (u_\tau - u_0)^2/\tau^2 + \mathcal{O}(u_\tau^{-1}). \quad (57)$$

For the action Eqs. (45) or (52) apply, depending on the sign of u_τ . Expansion in terms of H yields σ_- to be of order $\mathcal{O}(H^{-1})$ so that

$$S(u_0, u_\tau, \tau, H) = 2(1 + H)\tau + 2 \ln \left(\frac{\cosh(u_\tau)}{\cosh(u_0)} \right) + \mathcal{O}(H^{-1}). \quad (58)$$

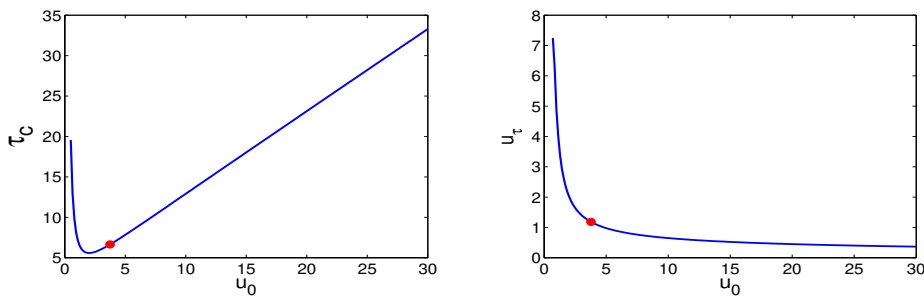


FIG. 12: (Color online) Time τ_c and position u_τ for the emergence of the kink in the minimised action as a function of the initial condition u_0 (see Eqs. (60)). The filled circle indicates the starting point of the kink for $u_0 = 4$, as in Fig. 7(c).

Hence, using Eq. (57) we end up with

$$S(u_0, u_\tau, \tau, H) = \frac{(u_\tau - u_0)^2}{\tau} + \tau + 2 \ln \left(\frac{\cosh(u_\tau)}{\cosh(u_0)} \right) + \mathcal{O}(u_\tau^{-1}). \quad (59)$$

To leading order, the tails of the propagator have a Gaussian shape, as expected, while the subleading terms indicate a transition from the Gaussian shape to the exponential shape of the stationary distribution.

3. Emergence and propagation of the kink

As mentioned before, a kink in the minimised action appears when the energy-time relation has multivalued inverse. Since $\theta_-(u_0, u_\tau, \tau, H)$ is a monotonic decreasing function of H , the kink appears when $\theta_+(u_0, u_\tau, \tau, H)$ develops a crossover from a monotonic increasing shape into a cubic shape (see Fig. 10(b,c)). Hence, the time τ_c when the kink appears and its position u_τ as a function of initial position u_0 are determined by

$$\tau = \theta_+(u_0, u_\tau, H), \quad \frac{\partial \theta_+}{\partial H} = 0, \quad \frac{\partial^2 \theta_+}{\partial H^2} = 0. \quad (60)$$

Figure 12 shows the solution of these equations. For small values of u_0 , i.e., in the limiting case of the Ornstein-Uhlenbeck process, both the time and the position for the emergence of the kink become large. For large values of u_0 , i.e., when the drift is almost constant, the time becomes large again but the kink appears close to the origin. At an intermediate scale of the size of the regularisation length the time for the occurrence of the kink becomes minimal, and the kink appears close to the initial condition.

After its appearance the kink starts to move with positive velocity (see Fig. 11(b) and Fig. 7(c)). We can quantify such a dynamical feature in terms of an asymptotic expansion for large τ and large u_τ , keeping the ratio $c = u_\tau/\tau$ of order $\mathcal{O}(1)$. Key to the analysis is the shape of the energy-time relation in such a limit (see Fig. 13).

The relation consists of the monotonic lower branch, Eq. (51), determined by θ_- and a cubic shaped upper branch, Eq. (46), determined by θ_+ . Depending on the value of τ the action takes its minimum either on the lower branch at an energy H_- which stays of order $\mathcal{O}(1)$ or on the upper branch at an energy H_+ which tends to zero in the asymptotic limit considered here. Hence, Eqs. (51) and (46) yield

$$\tau = \theta_-(u_\tau, u_0, H_-) = \frac{u_\tau}{\sqrt{1 + 2H_-}} + \mathcal{O}(1), \quad (61)$$

$$\tau = \theta_+(u_\tau, u_0, H_+) = u_\tau + \ln(2 \sinh(u_0)) - \ln(-2H_+) + \mathcal{O}(\exp(-2u_\tau), H_+). \quad (62)$$

Both expressions are easily inverted to obtain

$$1 + 2H_- = (u_\tau/\tau)^2 + \mathcal{O}(\tau^{-1}) \quad (63)$$

and

$$-2H_+ = 2 \sinh(u_0) \exp(u_\tau - \tau) (1 + \mathcal{O}(\exp(-2u_\tau), \exp(-\tau(1 - c)))) , \quad (c = u_\tau/\tau < 1), \quad (64)$$

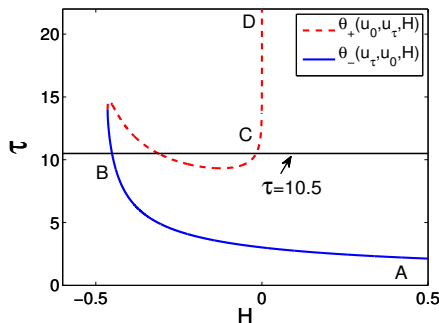


FIG. 13: (Color online) Energy time relation, Eqs. (51) and (46) for $u_0 = 2$ and $u_\tau = 5$. The action takes its minimum on the lower branch AB if $\tau < 10.5$ and on the upper branch CD if $\tau > 10.5$.

where for Eq. (64) we have to require that $c = u_\tau/\tau < 1$. Otherwise the matching condition for the action cannot be met since the branch θ_+ has a minimum at finite time (see Fig. 13).

As for the value of the action along the lower branch Eq. (52) yields, if we observe that σ_- is of order $\mathcal{O}(1)$,

$$S_- = 2(1 + H_-)\tau + 2u_\tau + \mathcal{O}(1) = \tau \left(\frac{u_\tau}{\tau} + 1 \right)^2 + \mathcal{O}(1), \quad (65)$$

where we have used Eq. (63) as well. For the action along the upper branch, Eq. (50), we have to take into account that σ_+ can be expressed as $-\ln(-2H_+) + \mathcal{O}(1)$ so that

$$S_+ = 2\tau + 2u_\tau + 2\ln(-2H_+) + \mathcal{O}(1) = 4u_\tau + \mathcal{O}(1), \quad (66)$$

where we have employed Eq. (64). The kink's position is determined by equating the expressions (65) and (66), resulting in $u_\tau = \tau$, so that the kink moves with unit speed. Finally, the minimised action to lowest order reads

$$S = \begin{cases} 4u_\tau, & \text{if } u_\tau < \tau, \\ \tau(u_\tau/\tau + 1)^2, & \text{if } u_\tau > \tau, \end{cases} \quad (67)$$

which indeed describes the numerical findings shown in Fig. 7.

V. CONCLUSION

We have studied in this paper a piecewise constant SDE in order to understand to which extent saddle-point approximations of the path integral representation of the propagator, which is the basis of weak noise approximations, can be carried out. The advantage of the SDE that we have considered is that its propagator is known exactly, so that any saddle-point approximations can be compared to the exact result.

For this model, we have seen that saddle-point approximations are able to reproduce some features of the propagator, such as its tail behaviour and its convergence towards the stationary distribution, but not the bimodality of the exact propagator appearing at intermediate times. We have also seen that the lowest-order approximation yields the correct large deviation approximation of the propagator, implying that the low-noise large deviation theory of Freidlin-Wentzell can be applied to this singular SDE. However, the construction of higher-order corrections to this approximation is plagued by a fundamental singularity of the Jacobian term of the path integral.

To remove this singularity, we have regularised the discontinuity of the SDE with a smooth nonlinear drift involving a small parameter controlling the limit to the piecewise smooth drift. The price paid for introducing this regularisation is that the two limits, small diffusion and small regularisation, do not commute and that the propagator of the regularised SDE is no longer known exactly. Nevertheless, we have shown with simulation results that the small noise limit of the regularised SDE captures the main features of the piecewise smooth SDE. In particular, the orbit or optimal path structure of the regularised SDE in terms of direct, indirect and intermediate paths is similar to the optimal path structure inferred heuristically for the piecewise smooth SDE. In addition, the analysis of the regularised SDE justifies the heuristic principles that we have defined and used to perform the saddle-point approximation of the piecewise smooth SDE. For the regularised SDE considered here, we have finally been able to study the quasi-potential associated with the propagator in a largely analytical way. This is one of the few models for which such results can be obtained. In a future study, we will consider higher-dimensional systems, such as models in which inertia is present.

Acknowledgments

YC is supported by the Chinese Scholarship Council, the Hunan Provincial Innovation Foundation for Postgraduates (grant No. CX2011B011), and NUDT's Innovation Foundation (grant No. B110205). WJ gratefully acknowledges support from EPSRC through grant No. EP/H04812X/1, SFB910, and the kind hospitality by Eckehard Schöll and his group during a stay at TU Berlin.

APPENDIX A: WEAK NOISE APPROXIMATION OF PATH INTEGRALS

Path integral formulations of the propagator of SDEs and their expansion for weak noise are well established in the literature. To set the notation and to keep the presentation self-contained, we summarise here the essential features, following the formulation presented in [31]. Let us consider the one-dimensional Langevin equation

$$\dot{v} = -f(v) + \sqrt{D}\xi(t), \quad (\text{A1})$$

where $f(v)$ is a smooth right hand side and the Gaussian white noise $\xi(t)$ obeys Eq. (2). We can write down the conditional probability $p(v_t, t|v_0, 0)$ by using the path integral formula [31],

$$p(v_t, t|v_0, 0) = \int_{(v_0, 0)}^{(v_t, t)} \mathcal{D}[v] J[v] e^{-\frac{1}{4D} \int_0^t (\dot{v} + f(v))^2 ds} \quad (\text{A2})$$

where $\int \mathcal{D}v$ denotes the Wiener measure and the Jacobian term

$$J[v] = \exp\left(\frac{1}{2} \int_0^t f'(v) ds\right) \quad (\text{A3})$$

originates from a transformation $\xi(t) \rightarrow v(t)$. Putting the two exponentials together, we thus express the kernel of the path integral in terms of the action

$$S[v] = \int_0^t L(v(s), \dot{v}(s)) ds = \int_0^t ((\dot{v}(s) + f(v(s)))^2 - 2Df'(v(s))) ds. \quad (\text{A4})$$

All trajectories contribute to the path integral (A2), but for small D , the largest contribution will come from the trajectory with smallest action. At lowest order in D , this contribution is found by minimising the action

$$S^{(0)}[v] = \int_0^t (\dot{v}(s) + f(v(s)))^2 ds, \quad (\text{A5})$$

which does not take the contribution of Jacobian into account since it is multiplied by D . The corresponding boundary value problem determined by the Euler-Lagrange equation reads

$$\ddot{v}^{(0)}(s) = f(v^{(0)}(s))f'(v^{(0)}(s)), \quad v^{(0)}(0) = v_0, \quad v^{(0)}(t) = v_t. \quad (\text{A6})$$

Given the path minimising the action (A5), the leading order approximation of the propagator is thus given by

$$p^{(0)}(v_t, t|v_0, 0) = N_1 \exp(-S^{(0)}[v^{(0)}]/(4D)), \quad (\text{A7})$$

where the (time dependent) normalisation N_1 can be computed a posteriori.

To improve this approximation, one can construct asymptotic series expansions of the action, which do not, however, always ensure positivity of the propagator. A simpler way to improve on the approximation (A7) is to evaluate the action of Eq. (A4) with the Jacobian using the optimal path $v^{(0)}$; see Eq. (A6). This leads to the expression

$$p^{(0;1)}(v_t, t|v_0, 0) = N_2 \exp(-S[v^{(0)}]/(4D)). \quad (\text{A8})$$

A more coherent approach, perhaps, which keeps the spirit of the saddle-point approximation and ensures positivity of the propagator, is to evaluate the minimising path with the Jacobian, leading to the following Euler-Lagrange equation:

$$\ddot{v}^{(1)}(s) = f(v^{(1)}(s))f'(v^{(1)}(s)) - Df''(v^{(1)}(s)), \quad v^{(1)}(0) = v_0, \quad v^{(1)}(t) = v_t. \quad (\text{A9})$$

In this case, the corresponding first order expression for the propagator is given by

$$p^{(1)}(v_t, t|v_0, 0) = N_3 \exp(-S[v^{(1)}]/(4D)). \quad (\text{A10})$$

In general, it is not possible to solve the boundary value problem of the Euler-Lagrange equations (A6) or (A9) analytically. Hence, numerical methods such as the shooting method must be used. In this case, it is useful to respect the underlying Hamiltonian structure of the Euler-Lagrange problem by using symplectic integration methods which preserve the Hamiltonian,

$$H^{(0)}(v, p_v) = p_v^2/2 - f^2(v)/2 \quad (\text{A11})$$

without the Jacobian or

$$H(v, p_v) = p_v^2/2 - (f^2(v) + Df'(v))/2 \quad (\text{A12})$$

with the Jacobian. In this case, a symplectic Euler scheme or the Störmer-Verlet scheme, for example, can be applied to integrate the corresponding canonical equations of motion.

APPENDIX B: ENERGY-TIME RELATION

1. Monotonicity of θ_-

Consider the expression defined in Eq. (42) either for $u_\tau < 0 < u_0$ and $H > 0$, or for $0 < u_\tau < u_0$ and $H > H_{min} = -\tanh^2(u_\tau)/2$. The argument of the logarithm in Eq. (42) can be written as

$$g(x) = \frac{a + \sqrt{x + a^2}}{b + \sqrt{x + b^2}} \quad (\text{B1})$$

and it is easy to see that $g(x) > 1$ in the given parameter ranges, i.e. either $b < 0 < a$ and $x > 0$, or $0 < b < a$ and $x > -b^2$. In addition, it follows by differentiation that $g'(x) < 0$, i.e., g is monotonic decreasing. Hence, θ_- considered as a function of H is the product of two positive monotonic decreasing functions, so that θ_- itself is monotonic decreasing.

2. Critical points of θ_+

Since Eq. (47) is a symmetric expression in the first two arguments it is sufficient to consider the case $0 < u_\tau < u_0$ and $H_{min} = -\tanh^2(u_\tau)/2 < H < 0$. The critical points are determined by the vanishing derivative of θ_+ . It is more convenient to consider the expression in terms of the new variable $\chi \in [0, u_\tau]$ defined by $H = -\tanh^2(\chi)/2$, where $-\chi$ represents the turning point of the indirect path, introduced in Section IV A 2. Then differentiation gives

$$\frac{\partial \theta_+(u_0, u_\tau, -\tanh^2(\chi)/2)}{\partial \chi} = h(\sinh(u_0), \sinh(\chi)) + h(\sinh(u_\tau), \sinh(\chi)), \quad (\text{B2})$$

where we have introduced

$$h(a, z) = z \ln \left(a/z + \sqrt{(a/z)^2 - 1} \right) - \frac{(1 + z^2)a}{z\sqrt{a^2 - z^2}}, \quad (0 < z < a). \quad (\text{B3})$$

The critical points of θ_+ are thus determined by the solutions of the equation

$$h(\sinh(u_0), z) + h(\sinh(u_\tau), z) = 0. \quad (\text{B4})$$

We now show that the right-hand side of Eq. (B2) is a convex function of $z = \sinh(\chi)$, so that there exist at most two solutions. To do so, compute the second derivative of Eq. (B3):

$$\frac{\partial h(a, z)}{\partial z} = \ln \left(a/z + \sqrt{(a/z)^2 - 1} \right) + a \frac{z^4 - 2(a^2 + 1)z^2 + a^2}{z^2(a^2 - z^2)^{3/2}} \quad (\text{B5})$$

and

$$\frac{\partial^2 h(a, z)}{\partial z^2} = -a \frac{z^4(6 + 2a^2) + z^2(-5a^2 + a^4) + 2a^4}{z^3(a^2 - z^2)^{5/2}}. \quad (\text{B6})$$

It is easy to see that the numerator in Eq. (B6) is positive by completing the square $6(z^2 - a^2/2)^2$. Hence, the second derivative is negative for any (positive) values of a . The same holds for Eq. (B4), proving convexity.

Finally, it is obvious from Eq. (47) that $\theta_+(u_0, u_\tau, H)$ tends to ∞ as $H \uparrow 0$ and that $\theta_+(u_0, u_\tau, H_{min})$ is finite and positive, resulting altogether in a cubic shape for the graph of $\theta_+(u_0, u_\tau, H)$.

* Electronic address: yaming.chen@qmul.ac.uk

† Electronic address: a.baule@qmul.ac.uk

‡ Electronic address: htouchet@alum.mit.edu

§ Electronic address: w.just@qmul.ac.uk

- [1] A. F. Filippov, *Differential Equations with Discontinuous Righthand Sides* (Kluwer, Dordrecht, 1988).
- [2] M. di Bernardo, C. Budd, A. Champneys, and P. Kowalczyk, *Piecewise-Smooth Dynamical Systems: Theory and Applications* (Springer, Berlin, 2008).
- [3] O. Makarenkov and J. S. W. Lamb, *Physica D* **241**, 1826 (2012).
- [4] B. J. J. Biemond, N. van de Wouw, and H. Nijmeijer, *Physica D* **241**, 1882 (2012).
- [5] A. Colombo, M. di Bernardo, S. J. Hogan, and M. R. Jeffrey, *Physica D* **241**, 1845 (2012).
- [6] F. P. Bowden and D. Tabor, *Friction and Lubrication of Solids* (Oxford University Press, Oxford, 1950).
- [7] F.-J. Elmer, *J. Phys. A: Math. Gen.* **30** (1997).
- [8] B. N. J. Persson, *Sliding Friction: Physical Principles and Applications* (Springer, Berlin, 1998).
- [9] E. J. Berger, *Appl. Mech. Rev.* **55**, 535 (2002).
- [10] M. R. Jeffrey, *Phys. Rev. Lett.* **106**, 254103 (2011).
- [11] P. Reimann, *Phys. Rep.* **361**, 57 (2002).
- [12] T. K. Caughey and J. K. Dienes, *J. Appl. Phys.* **32**, 2476 (1961).
- [13] J. D. Atkinson and T. K. Caughey, *Int. J. Non-Linear Mech.* **3**, 399 (1968).
- [14] P.-G. de Gennes, *J. Stat. Phys.* **119**, 953 (2005).
- [15] H. Hayakawa, *Physica D* **205**, 48 (2005).
- [16] A. Baule and P. Sollich, *Europhys. Lett.* **97**, 20001 (2012).
- [17] H. Touchette, E. V. der Straeten, and W. Just, *J. Phys. A: Math. Theor.* **43**, 445002 (2010).
- [18] M. K. Chaudhury and S. Mettu, *Langmuir* **24**, 6128 (2008).
- [19] P. S. Goohpattader, S. Mettu, and M. K. Chaudhury, *Langmuir* **25**, 9969 (2009).
- [20] P. S. Goohpattader and M. K. Chaudhury, *J. Chem. Phys.* **133**, 024702 (2010).
- [21] A. Gnoli, A. Puglisi, and H. Touchette, *Europhys. Lett.* **102**, 14002 (2013).
- [22] D. J. W. Simpson and R. Kuske, arXiv:1204.5792 (2012).
- [23] I. Karatzas and S. E. Shreve, *Ann. Prob.* **12**, 819 (1984).
- [24] W. Zhang, *IEEE Trans. Aut. Cont.* **35**, 980 (1990).
- [25] V. E. Benes, L. A. Shepp, and H. S. Witsenhausen, *Stochastics* **4**, 39 (1980).
- [26] S. Browne and W. Whitt, in *Advances in Queueing*, edited by J. Dshalalow (CRC Press, Boca Raton, FL, 1995), pp. 463–480.
- [27] M. Gradinaru, S. Herrmann, and B. Roynette, *Ann. Inst. Poincaré B* **37**, 555 (2001).
- [28] A. P. Korostelev and S. L. Leonov, *Prob. Th. Rel. Fields* **94**, 317 (1993).
- [29] T.-S. Chiang and S.-J. Sheu, *Ann. Prob.* **28**, 140 (2000).
- [30] M. Boué, P. Dupuis, and R. S. Ellis, *Prob. Th. Rel. Fields* **116**, 125 (2000).
- [31] M. Chaichian and A. Demichev, *Path Pntegrals in Physics: Stochastic Processes and Quantum Mechanics*, vol. 1 (IOP, London, 2001).
- [32] R. Graham, in *Noise in Nonlinear Dynamical Systems*, edited by F. Moss and P. V. E. McClintock (Cambridge University Press, Cambridge, 1989), vol. 1, pp. 225–278.
- [33] H. Touchette, *Phys. Rep.* **478**, 1 (2009).
- [34] A. Baule, E. G. D. Cohen, and H. Touchette, *J. Phys. A: Math. Theor.* **43**, 025003 (2010).
- [35] A. Baule, H. Touchette, and E. G. D. Cohen, *Nonlinearity* **24**, 351 (2011).
- [36] M. I. Freidlin and A. D. Wentzell, *Random Perturbations of Dynamical Systems*, vol. 260 of *Grundlehren der Mathematischen Wissenschaften* (Springer-Verlag, New York, 1984).
- [37] P. Kloeden and E. Platen, *Numerical Solution of Stochastic Differential Equations* (Springer, Berlin, 1992).
- [38] R. Graham and T. Tél, *Phys. Rev. A* **31**, 1109 (1985).
- [39] W. Cassing and J. Knoll, *Phys. Lett. B* **106**, 443 (1981).